ACS OMEGA

Open Access

http://pubs.acs.org/journal/acsodf

Article

Efficient Adsorbent Derived from Phytolith-Rich Ore for Removal of Tetracycline in Wastewater

Xi Liu, Yili Tang, Xianguang Wang, Muhammad Tariq Sarwar, Xiaoguang Zhao, Juan Liao, Jun Zhang, and Huaming Yang*

Cite This: *ACS Omega* 2024, 9, 8287−8296

Read Online

ACCESS | Metrics & More | Article Recommendations | Supporting Information

ABSTRACT: In recent decades, the tetracycline (TC) concentration in aquatic ecosystems has gradually increased, leading to water pollution problems. Various mineral adsorbents for the removal of tetracyclines have garnered considerable attention. However, efficient adsorbents suitable for use in a wide pH range environment have rarely been reported. Herein, a phytolith-rich adsorbent (PRADS) was prepared by a simple one-step alkali-activated pyrolysis treatment using phytolith as a raw material for effectively removing TC. PRADS, benefiting from its porous structure, which consists of acid- and alkali-resistant, fast-adsorbing macroporous silica and mesoporous carbon, is highly desirable for efficient TC removal from wastewater. The results indicate that PRADS exhibited excellent adsorption performance and stability for TC over a wide pH range of 2.0−12.0 under the coexistence of competing ions, which could be attributed to the fact that PRADS has a porous structure and contains abundant oxygen-containing functional groups and a large number of bonding sites. The adsorption mechanisms of PRADS for TC were mainly attributed to pore filling, hydrogen bonding, $\pi-\pi$ electron-donor−acceptor, and electrostatic interactions. This work could offer a novel preparation strategy for the effective adsorption of pollutants by new functionalized phytolith adsorbents.

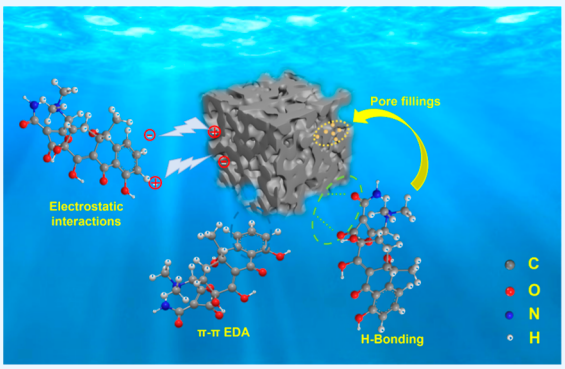

INTRODUCTION

Tetracycline (TC), a common antibiotic with low cost and high consumption, cannot be fully metabolized or removed from the environment.[1] Concentrations in shallow groundwater were measured at 184.2 ng/L,[2] and TC levels detected in aquatic environmental matrices ranged from 1.1 ng/L to 12 mg/L.[3] Domestic wastewater contained less TC than wastewater released from pharmaceutical plants and aquaculture farms.[4] These environmental compounds pose a significant risk to human health and ecological integrity.[5] Consequently, removing TC from natural water and wastewater has drawn increasing attention to environmental and health issues. Several methods have been developed to remove organic pollutants from wastewater,[6] for instance, adsorption, advanced oxidation processes (AOP),[7] biological methods,[8,9] membrane separations,[10,11] and so on. Although the AOP method is clean and environmentally friendly, it is difficult and costly to operate and is insufficient to purify wastewater completely. In addition, the decomposition products of the AOP method may still be biotoxic.[12−14] Biological methods are also limited by long remediation cycles and additional energy consumption by microorganisms.[15] The membrane separation method's main disadvantage is its relatively low separation efficiency due to its application scenario, surfactant leakage, and susceptibility to fouling.[16] Compared to the other methods, the adsorption method is recognized as the most cost-effective and practical method for water remediation due to its simple operational design, low investment and operating costs, and high removal efficiency.[17] Various adsorbents have been developed for the adsorptive removal of TCs, such as biochar,[18] mineral materials,[19] nanomaterials,[20] and metal skeleton organics.[21] However, conventional adsorbents still suffer from pH, temperature, and low adsorption capacity to remove TC molecules. Therefore, it is crucial to develop a method applicable over a wide range of pH and temperature values, which could efficiently and inexpensively remove TC from wastewater.

Recently, natural minerals such as kaolin and montmorillonite have been commonly used for tetracycline adsorption due to their excellent biocompatibility, efficient adsorption, and wide distribution.[22,23] SiO_2, as a kind of metalloid, usually exists in the form of a silicic acid polymer, presenting a 3D structure of Si−O connection containing siloxane (Si−O−Si)

Received: November 13, 2023
Revised: January 25, 2024
Accepted: January 26, 2024
Published: February 7, 2024

and silanol (Si−OH). There are also abundant hydroxyl groups on the surface of SiO_2. Accordingly, they react strongly with other substances, and the application performance is excellent.[24] Biochar is a stabilized carbon matrix with a porous structure that offers exceptional physicochemical properties, including large specific surface area (SSA) and aromaticity, as well as economic advantages and sustainability.[25] Biochar is widely used for the preparation of adsorbents; however, its carbonization process often leads to the production of pollutant gases.[26] Phytolith is a noncrystalline mineral in living plants through silica deposition of cell walls, fillings of cell lumen, and intercellular spaces of the cortex near evaporating surfaces within plant tissue when the roots absorb dissolved silicon (monomeric silicic acid).[27,28] Phytolith in plants has been shown to have the potential for phytoremediation of soils.[29] Phytolith is composed mainly of silica with a small amount of carbon, which combines the benefits of silica and biochar as adsorbents. Thus, phytoliths can be used as suitable raw materials for the preparation of minerals and biomass adsorbents.

Appropriate modifications can further improve the physicochemical properties of the pristine adsorbents. Alkali treatment is a common method to change the surface properties of adsorbents. Owing to the advantages of low cost, environmental friendliness, high recovery rate, and the ability to form mesoporous structures, the surface area increased through synergistic interactions. NaOH promoted the activation process with a large number of functional groups (mainly −OH) and basicity through carbon−oxygen bonding.[30−32]

This work aimed to prepare an effective adsorbent by a simple NaOH alkaline activation one-step method using phytolith. The obtained synthetic porous phytolith-rich adsorbent (PRADS) exhibits a disordered and defective structure. The effects of activation temperature, initial solution pH, and coexisting ions on TC removal were also investigated. The kinetic and thermodynamic properties and corresponding mechanisms of TC removal by adsorbents are also presented. The current study provides experimental evidence to inform the development of high-performance functional adsorbents derived from phytolith biomass for TC removal.

RESULTS AND DISCUSSION

Adsorbent Preparation and Characterization. PRADS was prepared by a simple one-step alkali-activated pyrolysis treatment (NaOH, 900 °C) using phytolith as a raw material to remove TC effectively (Figure 1a). A series of experiments were designed to investigate the effects of the phytolith to NaOH weight ratio and calcination temperature on the adsorption performance during the alkali activation preparation of the materials. As can be seen from Figure S1, when the mass ratio of phytoliths to NaOH changed from 1:0.75 to 1:2, the removal rate of TC by the material showed an increasing trend, but when the mass ratio was greater than 1:1, the difference was not significant, and the optimal mass ratio of phytoliths to NaOH mass ratio was determined to be 1:1, taking into account the economic practicability. Figure S2 shows the weak removal of raw ore when the calcination temperature was increased from 300 to 900 °C and then to 1000 °C. The removal of TC by the material showed an increasing and then decreasing trend, so the optimum calcination temperature was determined to be 900 °C. Heat treatment temperature is the first and most important factor

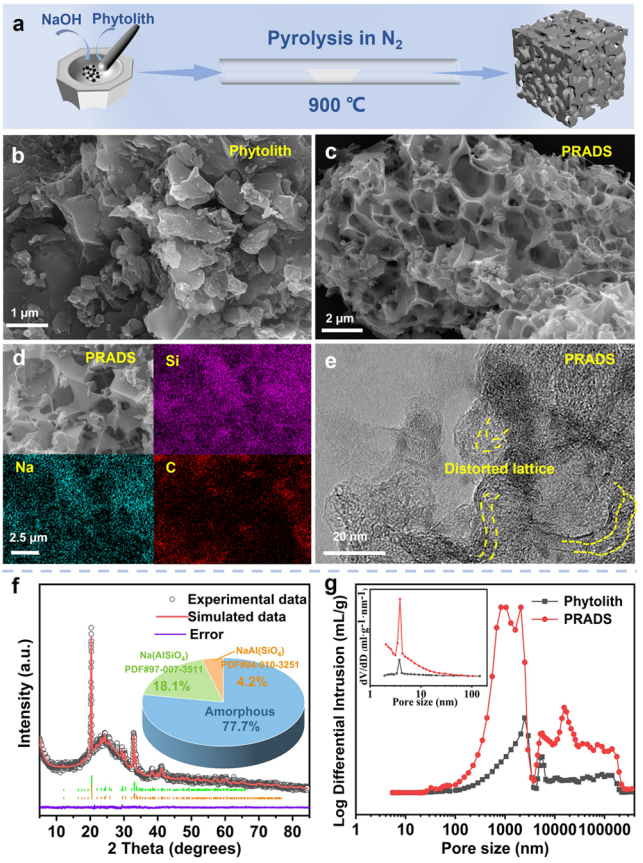

Figure 1. (a) Schematic illustrating the production of porous adsorbents. (b) SEM images of phytolith. (c) SEM images of PRADS. (d) Mapping of PRADS. (e) TEM images of PRADS. (f) Rietveld refinement results of the XRD data for PRADS. (g) Pore size distribution of pristine phytolith and PRADS.

affecting the pore development of carbonaceous materials. Figure S3 shows that when the calcination temperature is increased to 600 °C, the material starts to show a pore structure, and when the temperature is increased to 900 °C, a clear macroporous structure appears on the surface, which indicates enhanced exposed surface area and pore size, and when it goes to 1000 °C, the pore structure collapses due to overreaction, which naturally results in the adsorption capacity of the TC decrease.

Scanning electron microscopy (SEM) images showed that the phytolith was lamellar (Figure 1b) and formed a distinct porous structure after activation by NaOH (Figure 1c). Figure 1d shows that the macroporous ones are silicon structures and the microporous and mesoporous ones are carbon structures. Lattice distortions of the samples are observed in Figure 1e, and these distortions indicate that there are intrinsic defects in the PRADS samples with an increase in the level of defective carbon. NaOH is well-known as an effective activation precursor for disordered carbon materials. The alkali activation method aids in increasing porosity and clearing up partially blocked pores of phytolith and increasing activated surface area and adsorption capacity.[33] The resulting XRD pattern is shown in Figure 1f, and Rietveld refinement of the powder XRD data was performed by the computer program Jade 9.0. Two main structures (Na ($AlSiO_4$): PDF#97-007-3511 and NaAl (SiO_4): PDF#04-010-3251) were used. The amorphous phase content was calculated to be 77.6%, and the crystalline phases of the

https://doi.org/10.1021/acsomega.3c09049
ACS Omega 2024, 9, 8287−8296

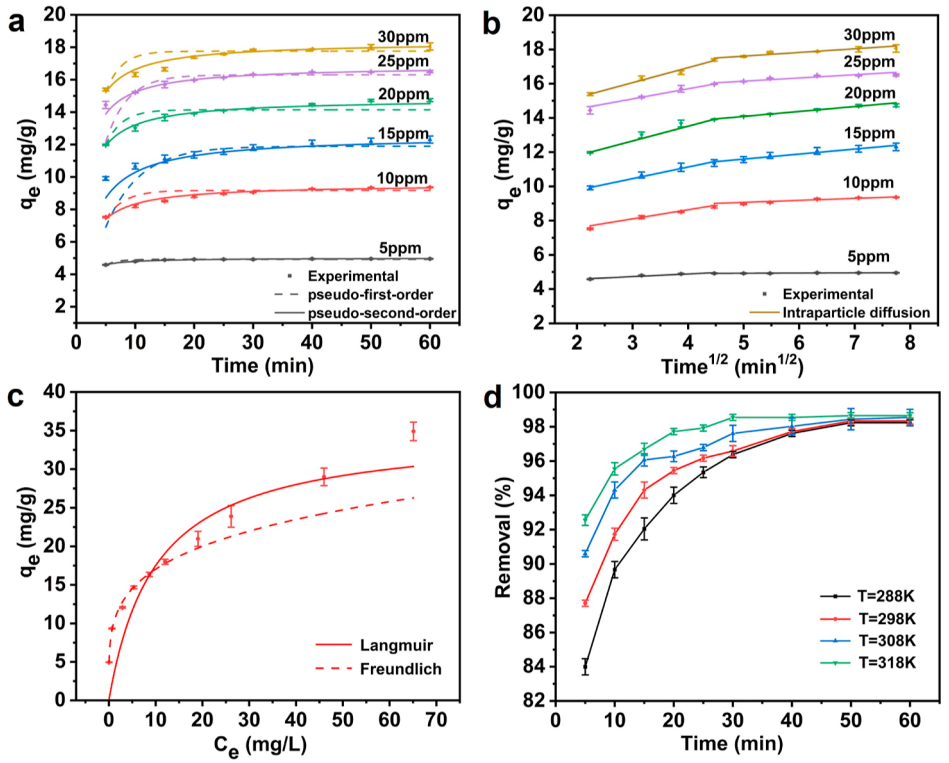

Figure 2. (a) Fitting to the pseudo-first-order and pseudo-second-order models of PRADS. (b) Fitting to the intraparticle diffusion of PRADS. (c) Equilibrium adsorption isotherms fitted by the Langmuir and Freundlich models. (d) Adsorption isotherms of TC at different temperatures on PRADS.

two types of sodium aluminum silicate were 18.1 and 4.2%, respectively. The calculated details of the XRD refinement are shown in Figure S4 with R = 5.77%, E = 4.92%, and R/E = 1.17. Figure 1g shows that PRADS mesopores and macropores increased and are porous structures. Figure S5 shows that the sample shows a type IV adsorption isotherm with an H3 type hysteresis loop in the middle section, a capillary coalescence system appearing for porous adsorbents. Table S1 shows that the SSA of phytolith is enlarged from 5.859 to 60.233 m^2/g.

The FTIR in Figure S6 shows that most of the peaks disappeared after NaOH activation, which confirms the reduction reaction of functional groups on the surface of the phytolith after alkali modification. Consistent with that reported by Nguyen et al. (2021), aromatic groups that existed in the phytolith were characterized by the C═C vibrations at 1575 cm^{-1}, indicating organic matter remaining on the surface of phytolith. The vibration of Si identified the silica phase Si−O−Si bonds at 1026 cm^{-1} (asymmetric stretching) and 771 cm^{-1} (symmetric stretching).[34] Zeta potentials show the potential of the material at different pH values. pH_{PZC} decreases from 6.77 to 2.32, indicating that PRADS shows negative potential values in both the broad region of pH and the negative value increases with increasing pH (Figure S7). The X-ray photoelectron spectroscopy (XPS) spectrum in Figure S8 shows an increase of the Na element in PRADS, which also proves the presence of sodium intercalation, which causes the carbon lattice to swell and form some micropores.[1,30] XPS results in Figure S9 show an increase of sp^3-C defective carbon and an increase of oxygen-containing functional groups, which is favorable for the adsorption of TC.[35] After the alkali activation of the phytolith, the carbon was exposed and encapsulated on the surface of silicon, forming a macroporous silicon and mesoporous carbon structure. Meanwhile, the sodium intercalation caused the carbon lattice to expand, and some micropores formed.

Adsorption Behavior of PRADS. The adsorbent dosage affected the equilibrium adsorption capacity (Q_e) and adsorption rate (R) of TC. With the increase of PRADS dosage, the adsorption capacity (Q_e) showed a general decreasing trend, with a rapid decrease followed by a gradual decrease, and the removal rate of TC increased, with a rapid increase followed by a slow increase (Figure S10). Although the increase in PRADS dosage provided more adsorption sites for adsorption and increased the overall adsorption capacity, the total amount of TC adsorbed in solution was fixed, and the amount of adsorption dispersed per unit mass of adsorbent decreased with the increase in dosage.[36] As the dosage increased, the adsorption rate of TC from the samples increased at adsorption equilibrium. When the dosage of PRADS was increased from 0.5 to 1.0 g/L, the amount of TC adsorbed significantly increased, whereas when the amount of the addition was increased to 2.0 g/L, the amount of TC adsorbed increased only by a trace amount. Based on these experimental results, the PRADS dosage used in the subsequent experiments was set at 1.0 g/L, which resulted in a satisfactory removal rate and a good adsorption rate.

The adsorption results of PRADS are affected by the initial TC concentration. Figure 2a shows that the adsorption capacity for TC increases with the initial concentration.[37] This result is related to the driving force. Higher initial concentrations correspond to stronger driving forces that can be generated to overcome the mass transfer resistance between the solution and the adsorbent. However, the adsorption capacity of PRADS on TC was rapidly enhanced in the initial

https://doi.org/10.1021/acsomega.3c09049
ACS Omega 2024, 9, 8287−8296

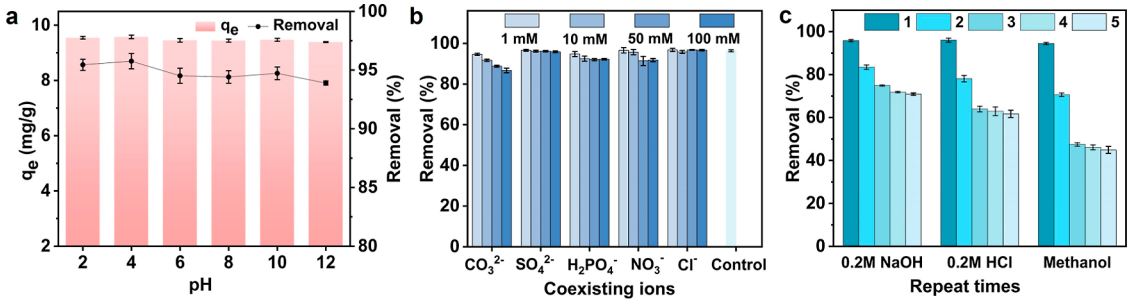

Figure 3. (a) Effects of pH on the adsorption of TC on PRADS. (b) Effect of coexisting ions on the adsorption performance of PRADS. (c) Recyclability of PRADS for adsorption of TC.

stage and slowly increased in the later stage. Although the adsorption capacity of PRADS increased with the initial TC concentration, the removal rates were reversed. Therefore, based on these results, the optimal initial concentration of TC was 10 mg/L.

The adsorption kinetics involving the adsorption mechanism and potential rate control phases were studied in detail (Figure 2a). Rapid adsorption was observed for the first 10 min, after which the adsorption rate gradually decreased. It is rapidly adsorbed on the surface in the initial phase and slowly diffused in the interior of the NPs in the second phase. The pseudo-first-order model and the pseudo-second-order model or the Weber intraparticle diffusion model were used to assess the adsorption process of TC.[38] The kinetic parameters are shown in Table S2. The R_2 values of all of the pseudo-second-order models are above 0.96, and the equilibrium adsorption amount (Q_e) is very close to the experimental data, indicating that the adsorption kinetics are consistent with the pseudo-second-order model.

The Weber intraparticle diffusion model was used to investigate the mechanism of adsorption kinetics further.[39] As can be seen from Figure 2b, none of the straight lines fitted by intraparticle diffusion passed through the origin of the coordinates, indicating that the adsorption rate is not controlled by Weber intraparticle diffusion alone and that the boundary layer diffusion effect also has some influence on the adsorption rate. From the fitted curves, the whole adsorption process can be divided into two linear stages. Stage 1 is the initial stage of adsorption. The adsorption process is mainly surface adsorption and boundary layer diffusion, and the adsorption rate is fast. As the adsorption reaction proceeds, stage 2 is intraparticle diffusion. As the concentration of tetracycline hydrochloride remaining in the solution decreases, there are fewer vacant sites on the surface of the adsorbent, and the molecules of tetracycline hydrochloride already adsorbed on the surface of the adsorbent diffuse into the interior of the PRADS particles, the rate of adsorption is slower, and the adsorption reaction reaches the equilibrium state gradually.

Table S3 shows the results of intraparticle diffusion fitting. The data show that the phase 1 diffusion rate constant $k_{p,1}$ value is higher than the phase 2 diffusion constant $k_{p,2}$ values. It indicates that with the prolongation of the adsorption reaction time, the pores on the surface of the PRADS adsorbent were occupied by a large number of tetracycline hydrochloride molecules and the adsorption rate of the adsorbent decreased. The nonzero C values for both phases indicate that intraparticle diffusion does not control adsorption during the kinetic process. Meanwhile, the constant C increases with increasing concentration, implying that the thickness of the boundary layer adsorption gradually increases with increasing concentration of tetracycline hydrochloride solution, and the influence of the boundary layer effect also increases.

The adsorption capacity of PRADS was enhanced with an increase of initial TC concentration (Figure 2c). This may be due to the prominent driving force provided by the high TC initial concentration, which controls the resistance to the transfer of adsorbate from the liquid fraction to the solid fraction in the adsorption system.[40] In order to investigate the adsorption behavior between TC and PRADS, two isotherm models, the Langmuir model and the Freundlich model, were used to fit the experimental data (Table S4). The Langmuir model assumes that the adsorbent has homogeneous sites, that adsorption is monolayer, and that there are no interactions between molecules and the adsorbent. The Langmuir fitted the experimental data well with the highest correlation coefficient (R_2 > 0.838), suggesting that the TC adsorption of PRADS may be monolayer and may be related to chemisorption. The bonding energy between TC molecules and the active sites on the adsorbent surface increased with an increase in temperature at different temperatures, and the Q_{max} and k_L parameters also increased. The separation factor known as dimensionless constant R_L was also recognized between 0 and 1, confirming the favorable adsorption process.[38]

The Freundlich model describes incompletely reversible adsorption involving the formation of multilayered adsorption layers on the PRADS, with the heat of adsorption and affinity distributed over a nonuniform surface.[26] The Freundlich model also fitted the experimental data well (R_2 > 0.988), indicating the presence of physisorption on the inhomogeneous surface of PRADS. The k_F value characterizing the amount of adsorption increases with increasing temperature. The nonhomogeneous factors $1/n$ describing the bond distributions are all less than 1, indicating that the PRADS surface has excellent adsorption affinity. In summary, the adsorption behaviors of TC on the surface of PRADS were physisorption and chemisorption, but physisorption was dominant.

Adsorption experiments at different temperatures (288, 298, 308, and 318 K) were carried out on the samples (Figure 2d). From the results of the thermodynamic parameters in Table S5, ΔG^0 is negative and ranges from −20 to 0 kJ·mol^{-1}, and the adsorption takes place mainly through physical interaction. The van der Waals force dominates the force, and the adsorption occurs mainly by spontaneous reaction.[41] Meanwhile, the absolute value of ΔG^0 increased with increasing temperature, but the increase was slight, indicating that the adsorption process was not affected much by temperature. ΔH^0

https://doi.org/10.1021/acsomega.3c09049
ACS Omega 2024, 9, 8287−8296

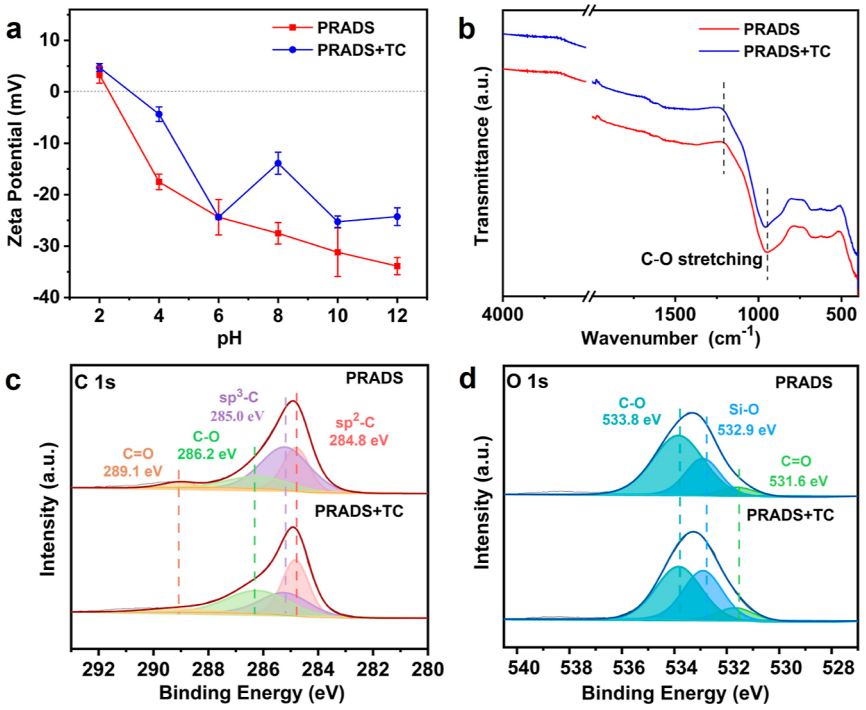

Figure 4. (a) Zeta potentials of PRADS and PRADS + TC at pH ranging from 2.0 to 12.0. (b) FTIR spectra of PRADS and PRADS + TC. (c) High-resolution C 1s spectrum of PRADS and PRADS + TC. (d) High-resolution O 1s spectrum of PRADS and PRADS + TC.

is less than 40 kJ·mol^{-1} and physical adsorption is dominant, indicating that the adsorption process is a heat-absorbing reaction. The ΔH^0 for the adsorption of tetracycline hydrochloride by PRADS was 7.178 kJ·mol^{-1}, indicating that the adsorption mechanism of tetracycline hydrochloride with PRADS was physisorption. The positive value of ΔS^0 indicates that the adsorption process is irreversible, and many tetracycline hydrochloride molecules are adsorbed on the surface of PRADS as the adsorption proceeds. The water molecules around tetracycline hydrochloride gradually decreased, the free water molecules increased, and the solid–liquid interface disorder increased.

Stability and Potential Application of PRADS. The initial pH of the solution was considered to be one of the critical factors affecting the adsorption process by changing the surface charge of the adsorbent to the present form of the adsorbate. TC is a hydrophilic amphiphilic molecule with a variety of functional groups, under different pH conditions. TC can exist in four different forms, namely, TCH^{3+} (pH < 3.3), TCH^0 (3.3 < pH < 7.7), TCH^- (7.7 < pH < 9.7), and TCH^{2-} (pH > 9.7). The surface charge of the adsorbent plays an important role in the removal of pollutants. Figure 3a shows that the removal of TC does not greatly vary for pH = 2–12, and the adsorbent is suitable for use in strongly acidic and alkaline environments. The pH_{pzc} of PRADS was 2.32, which indicated that the surface of PRADS was positive when the solution pH < 2.32, and the electrostatic repulsion between TCH^{3+} and PRADS inhibited the adsorption of TC. Similarly, when pH > 7.7, the surface of PRADS is negatively charged and between TCH^- and TC^{2-} is a strong electrostatic repulsion. In this case, the hydrogen and π bonds formed between TC and PRADS are the two main forces in the adsorption process. Overall, PRADS showed significantly superior TC adsorption capacity at all pH conditions, suggesting that electrostatic effects are negligible in the overall adsorption process.[42] In contrast, the adsorption capacity of many adsorbents for TC is severely limited by electrostatic repulsion.[43,44] PRADS samples achieved similar removal of TC in pure water (Figure 3a) and real water (tap water and Lake Donghu water) (Figure S11), suggesting its excellent adaptability in natural water. PRADS maintains a stable and excellent adsorption capacity over a wide pH range, which may give it an anti-interference advantage in environmental applications. The performance of other adsorbents is shown in Table S6, which can be compared to show that PRADS is suitable for a wide range of pH values and has a fast rate of adsorption, a short time to reach equilibrium, and effective adsorption.

Antibiotic production wastewater contains a large number of salts, and coexisting ions in the wastewater will compete with antibiotics for the adsorbent's adsorption sites, thus affecting the removal efficiency. This experiment explored the effect of common coexisting ions (CO_3^{2-}, SO_4^{2-}, $H_2PO_4^{2-}$, NO_3^-, Cl^-) on the adsorption of TC by PRADS. The mechanisms by which the strength of coexisting ions in solution affects the adsorption process include the following two ways.[45] The "extrusion" effect, i.e., the adsorption of antibiotics, decreases with increasing ionic concentration. The "extrusion effect", whereby ionic salts significantly affect antibiotics' conformational and electrostatic properties, decreases their solubility and thus affects their adsorption capacity. The results, as shown in Figure 3b, showed that SO_4^{2-}, $H_2PO_4^{2-}$, and Cl^- had a less inhibitory effect on the adsorption of TC, and CO_3^{2-} had a significant impact on its adsorption capacity. The main reason is that with the addition of Na_2CO_3, the pH of the solution increases, increasing the electrostatic repulsion between PRADS and TC. As the solubility of NO_3^- increases to 50 mM, the adsorption decreases slightly, known as the "extrusion effect".

https://doi.org/10.1021/acsomega.3c09049
ACS Omega 2024, 9, 8287–8296

In the practical application of adsorbents, recyclability is a crucial economic indicator, which reduces the cost of adsorbent use and the disposal cost of the waste adsorbent.[46] The key to recycling the adsorbent is to desorb and regenerate the adsorbent after use, so the regeneration effects of three desorption methods, namely, 0.2 M NaOH washing, 0.2 M dilute hydrochloric acid washing, and ethanol washing, were investigated. The results of cyclic adsorption−desorption experiments are shown in Figure 3c. After five cycles, PRADS maintained a high adsorption capacity, and the removal rates of the three adsorbents were 70.89, 61.71, and 44.89%, respectively, with the best desorption effect by the 0.2 M NaOH washing method. There was a certain decrease in adsorption after each cycle because TC occupied some of the adsorption sites of PRADS, and this irreversible adsorption may be related to chemisorption. The above-mentioned research demonstrated the feasibility of this route proposed in this work using a phytolith to prepare PRADS materials. Approximately 5 kg of phytoliths can prepare 1 kg of PRADS materials, where the process requires 5 kg of NaOH and 160 L of water. From a previous experimental study, we estimated that the total cost of the raw materials was about $ 35.116, and the total cost of energy consumption was about $ 112.43 (Table S7).

Adsorption Mechanisms of TC on PRADS. The mechanisms of TC adsorption included pore-filling, electrostatic interaction, surface complex interaction, hydrogen bonding, pore diffusion, and $\pi-\pi$ EDA interaction.[47,48] In this study, correlation analysis and characterization of biomass adsorbing TC were performed to investigate the mechanism of TC adsorption on a biomass adsorbent.

Figure S12 shows that TC pores were filled on the adsorbent, and the pores were reduced. Table S1 shows that after the adsorption of TC by PRADS, the surface area and pore volume were reduced, and the pore size was increased, indicating that the pore filling plays an essential role in the TC adsorption process. The carbon structure in PRADS promotes the formation of $\pi-\pi$ EDA interactions between the ring structure in the tetracycline molecule and the adsorbent carbon. Figure 4a shows the change in zeta potential before and after pH adsorption, and pH_{pzc} increased from 2.32 to 3.05, which indicates the presence of electrostatic interaction before and after adsorption. However, since excellent TC adsorption capacity was exhibited throughout the pH conditions, it indicated that the electrostatic effect during the whole adsorption process was weak and negligible. The blue shift of C−O stretching after TC adsorption in Figure 4b implied bond stabilization, which indicated that the material reacts with TC due to hydrogen bonding. The results indicate that hydrogen bonding is crucial in TC adsorption because C−O and C═O functional groups are essential for hydrogen bond formation. Similar results were reported in previous studies in which the C−O and C═O functional groups influenced the adsorption process in carbon.[49,50]

The significant increase in elemental N after adsorption is shown in Figures S13 and S14, indicating that TC is adsorbed on the adsorbent or reacted with the PRADS. In Figure S13, the intensity of C 1s was decreased due to the $\pi-\pi$ EDA effect. C 1s was divided into 4 peaks that correspond to binding energies of 284.8, 285.0, 286.2, and 289.1 eV, which are attributed to sp^2-C, sp^3-C, C−O, and O−C═O, respectively.[51] Figure 4c shows a reduction of sp^3-C defective carbon for the defective sites to be adsorbed, and the benzene ring structure in the TC molecule contains an aromatic solid structure that acts as an electron acceptor in the $\pi-\pi$ EDA process. Figure 4d shows the reduction of C−O and other oxygenated functional groups.

As a result, based on the comprehensive surface and structure analysis of the PRADS sample after TC adsorption, we speculate that several robust interactions (H-bond, electrostatic interaction, and $\pi-\pi$ EDA) and pore filling have improved the adsorption capacity of the PRADS sample (Figure 5).

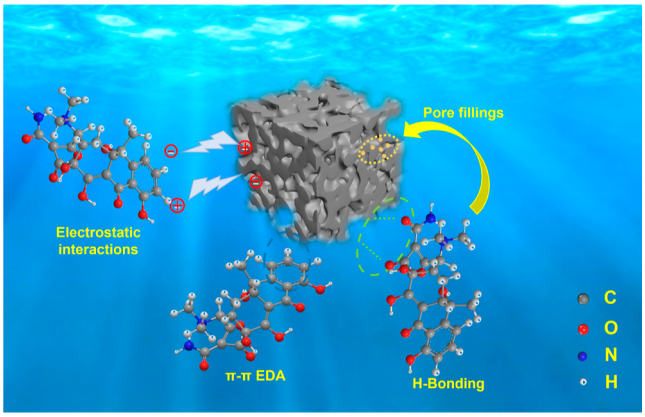

Figure 5. Adsorption mechanism of TC captured by PRADS.

CONCLUSIONS

We proposed a cost-effective and environmentally friendly technique for the preparation of phytolith-rich adsorbents (PRADS) for tetracycline antibiotics. The obtained PRADS with alkali activation treatment shows a greater SSA than phytolith-rich ore, a well-developed porosity, an abundance of oxygen-containing functional groups, and a vast number of bonding sites, which are beneficial for the adsorption of TC molecules. The adsorption kinetics results indicated that the adsorption process of PRADS to TC is mainly surface adsorption, boundary layer diffusion, followed by intraparticle diffusion, which fits well with the pseudo-second-order kinetics and the Langmuir isotherm model. The results of the adsorption isotherms showed that the surface adsorption of PRADS on TC was dominated by physisorption, accompanied by chemisorption. For adsorption performance, PRADS showed high stability and reusability in the presence of competing ions coexisting over a wide pH range (2.0−12.0). TC was presumed to be adsorbed on PRADS through pore filling, H-bond, electrostatic, and $\pi-\pi$ EDA interactions. In summary, PRADS could be regarded as a promising material for the adsorptive purification of TC-containing water under real-life conditions.

EXPERIMENTAL SECTION

Materials and Chemicals. The untreated phytolith-rich ore was produced from a mine in Fengcheng, Jiangxi, China, with a total carbon content of 132.96 ± 3.47 g/kg (Figure S15). Tetracycline (TC) was purchased from Macklin Inc. Shanghai, China. Sodium chloride (NaCl), sodium nitrate ($NaNO_3$), sodium sulfate (Na_2SO_4), sodium carbonate (Na_2CO_3), and sodium dihydrogen phosphate (NaH_2PO_4) were purchased from Aladdin Reagent Co. Ltd. (Shanghai, China). China National Pharmaceutical Chemical Reagent Co.

https://doi.org/10.1021/acsomega.3c09049
ACS Omega 2024, 9, 8287−8296

supplied sodium hydroxide (NaOH). These chemicals were used as received without further purification. Deionized water was used for TC adsorption experiments.

Preparation of the Adsorbent. Phytolith was mixed with NaOH in a mass ratio of 1:1 and then held in a tube furnace under a N_2 atmosphere at different temperatures with a heating rate of 10 °C/min for 2 h. Phytolith-rich adsorbents obtained from this activation process were designated as PRADS, which were washed several times with DI water until the pH value of the filtrate reached 7.0 ± 0.2, then kept in an oven at 80 °C for drying, and finally sealed in a container for further experimental use.

Adsorption Experiments. PRADS adsorption experiments on TC were carried out by adding PRADS to a 50 mL solution system at different temperatures. The mixture of PRADS and pollutants was rotated in a water bath for 2 h. The effects of adsorbent dosing, initial pollutant concentration, inorganic salt, pH, and recyclability were examined. Samples were taken at regular intervals, the solution passed through a 0.45 μm filter head, and the absorbance values were determined at 357 nm. The concentrations of TC (C_0 and C_e) in the adsorption system were calculated. The removal of TC by PRADS and the equilibrium adsorption Q_e were determined by eqs 1 and 2, respectively.

$$Q_e = \frac{(C_0 - C_e)V}{m} \tag{1}$$

$$R\ (\%) = \frac{(C_0 - C_e)}{C_0} \times 100\% \tag{2}$$

where Q_e (mg/g) is the equilibrium adsorption of TC by the adsorbent, C_0 (mg/L) and C_e (mg/L) are the initial and equilibrium concentrations of TC, respectively, V (mL) is the volume of TC solution, m (mg) is the amount of adsorbent, and R (%) is the adsorption rate of TC.

Characterization. The surface morphology of the sample was observed using a scanning electron microscope (Zeiss GeminiSEM 500, Germany); the elemental distribution was determined by an energy spectrometer (EDS, Oxford, X-Max), and the microstructure of the samples was investigated by transmission electron microscopy (TEM, FEI TF20, Germany). Changes in the phase composition of the adsorbent were investigated by using an X-ray diffractometer (Bruker Corp., Germany). XPS (ESCALAB Xi+, USA) and Fourier transform infrared spectroscopy (FTIR, BRUKER Tensor II, Germany) analyzed the chemical functional groups, elemental compositions, and bonding states. PRADS and pore distribution of the adsorbent were determined by a nitrogen adsorption−desorption method using a surface area analyzer (BET, ASAP 2020 Plus, Micromeritics, America). The zeta potential analysis of samples was determined using a Zeta potential Tester (Zetasizer NanoZS, Malvern, UK) at different solution pH (2.0−12.0).

Data Analysis. In order to better understand the adsorption process, two classical adsorption kinetic models, the pseudo-first-order model and the pseudo-second-order model, and two classical adsorption isotherm models, the Langmuir model and the Freundlich model, respectively, were used to fit the kinetic and isotherm studies as well as the Weber intraparticle diffusion model. The detailed equations for the above model are shown below.

The pseudo-first-order kinetics model

$$Q_t = Q_e(1-e^{k_1 t}) \tag{3}$$

The pseudo-second-order kinetics model

$$Q_t = \frac{k_2 Q_e{}^2 t}{1 + k_2 Q_e t} \tag{4}$$

The intra-particle diffusion kinetic model

$$Q_t = k_i t^{1/2} + C_i \tag{5}$$

where Q_e (mg·g^{-1}) is the equilibrium adsorption capacity; the adsorption rate constants k_1 (min^{-1}) and k_2 (g·(mg·min)$^{-1}$) are the quasi-first-order and quasi-second-order kinetics, respectively. k_i (mg·(g·min$^{1/2}$)$^{-1}$) is the diffusion rate constant within the particle. The constant C_i is associated with the thickness of the boundary layer.

The Langmuir model

$$Q_e = \frac{Q_m K_L C_e}{1 + K_L C_e} \tag{6}$$

The Freundlich model

$$Q_e = K_F C_e^{1/n} \tag{7}$$

where K_L (L mg^{-1}) and K_F (mg$^{(1-1/n)}$ L$^{1/n}$ g^{-1}) denote Langmuir and Freundlich constants, respectively. The parameter k_L is related to the affinity and adsorption energy of the adsorption site and the parameter K_F is related to the adsorption capacity.

$$\ln K_d = \frac{-\Delta H^\circ}{R \times T} + \frac{\Delta S^\circ}{R} \tag{8}$$

$$K_d = \frac{Q_e}{C_e} \tag{9}$$

$$\Delta G^\circ = -R \times T \times \ln K_d \tag{10}$$

where K_d (L·mol^{-1}) is the Freundlich isotherm constant, R is the ideal gas constant (8.314 J mol^{-1}·K^{-1}), and T is the temperature (K).

Reusability of Adsorbents. Adsorption experiments were carried out by adding 50 mg of PRADS to 50 mL of TC solution, recovering the used material, desorbing the material, drying it to continue the adsorption experiments, and repeating the cycle of adsorption−desorption experiments five times. The adsorbed PRADS was transferred to a beaker, and 50 mL of 0.2 M NaOH, 0.2 M HCl, and ethanol were added and placed in a water bath at 25 °C with stirring for washing and filtration, and the process was repeated five times with a stirring time of 30 min.

■ ASSOCIATED CONTENT

Supporting Information

The Supporting Information is available free of charge at https://pubs.acs.org/doi/.

TC adsorption capacity with different mass ratios of phytoliths to NaOH; TC adsorption capacity with different calcination temperatures; SEM images of different calcination temperatures; peak fit stops at the 25th iteration; N_2 adsorption/desorption isotherm curves of pristine phytolith and PRADS; FTIR spectra of phytolith and PRADS; zeta potentials of phytolith and PRADS at pH ranging from 2.0 to 12.0; XPS survey

https://doi.org/10.1021/acsomega.3c09049
ACS Omega 2024, 9, 8287−8296

spectra of phytolith and PRADS; high-resolution C 1s and O 1s spectra of phytolith and PRADS; effect of dosage on the removal efficiency of TC adsorption onto PRADS; effects of pH on the adsorption of TC on PRADS in tap water and Lake Donghu water; N_2 adsorption/desorption isotherm curves of PRADS and PRADS + TC; BJH pore size distribution curves of pristine PRADS and PRADS + TC; XPS survey spectra of PRADS and PRADS + TC; high-resolution N 1s spectra of phytolith, PRADS, PRADS + TC; XRD patterns of phytolith; pore structure characteristics of phytolith, PRADS, and PRADS + TC; adsorption kinetic parameters of pseudo-first-order and pseudo-second-order kinetic models for phosphate adsorption by PRADS; fitted parameters of the intraparticle diffusion model for TC adsorption on PRADS; adsorption isotherm parameters for phytolith adsorption by the samples; adsorption thermodynamic parameters of TC by PRADS; comparison of the TC adsorption capacities of different adsorbents in the literature; and price of raw materials and treatment energy consumption of the proposed methods (PDF)

AUTHOR INFORMATION

Corresponding Author

Huaming Yang − *Hunan Key Laboratory of Mineral Materials and Application, School of Minerals Processing and Bioengineering, Central South University, Changsha 410083, China; Engineering Research Center of Nano-Geomaterials of Ministry of Education, China University of Geosciences, Wuhan 430074, China; Laboratory of Advanced Mineral Materials and Faculty of Materials Science and Chemistry, China University of Geosciences, Wuhan 430074, China;* orcid.org/0000-0002-3097-2850; Phone: +86-27-68788701; Email: hm.yang@cug.edu.cn; Fax: +86-27-68788733

Authors

Xi Liu − *Hunan Key Laboratory of Mineral Materials and Application, School of Minerals Processing and Bioengineering, Central South University, Changsha 410083, China; Department of Natural Resources of Jiangxi Province, Jiangxi Province Natural Resources Interests and Reserve Security Center, Nanchang 330025, China*

Yili Tang − *Hunan Key Laboratory of Mineral Materials and Application, School of Minerals Processing and Bioengineering, Central South University, Changsha 410083, China*

Xianguang Wang − *Department of Natural Resources of Jiangxi Province, Jiangxi Mineral Resources Guarantee Service Center, Nanchang 330025, China*

Muhammad Tariq Sarwar − *Engineering Research Center of Nano-Geomaterials of Ministry of Education, China University of Geosciences, Wuhan 430074, China; Laboratory of Advanced Mineral Materials and Faculty of Materials Science and Chemistry, China University of Geosciences, Wuhan 430074, China*

Xiaoguang Zhao − *Hunan Key Laboratory of Mineral Materials and Application, School of Minerals Processing and Bioengineering, Central South University, Changsha 410083, China*

Juan Liao − *Hunan Key Laboratory of Mineral Materials and Application, School of Minerals Processing and Bioengineering, Central South University, Changsha 410083, China*

Jun Zhang − *Hunan Key Laboratory of Mineral Materials and Application, School of Minerals Processing and Bioengineering, Central South University, Changsha 410083, China*

Complete contact information is available at: https://pubs.acs.org/10.1021/acsomega.3c09049

Author Contributions

Huaming Yang conceived the project. Xi Liu wrote the initial drafts of the paper. Huaming Yang wrote the final paper. Xi Liu designed the experiments. Xi Liu and Yili Tang synthesized and characterized the materials. Xi Liu, Xianguang Wang, and Xiaoguang Zhao analyzed the data. Juan Liao, Muhammad Tariq Sarwar, and Jun Zhang carried out the formal analysis. All authors discussed the results and commented on the manuscript.

Notes

The authors declare no competing financial interest.

ACKNOWLEDGMENTS

This work was supported by the CUG Scholar Scientific Research Funds at China University of Geosciences (Wuhan) (2019152), the Fundamental Research Funds for the Central Universities at China University of Geosciences (Wuhan), and the National Science Fund for Distinguished Young Scholars (51225403).

REFERENCES

(1) Wei, M.; Marrakchi, F.; Yuan, C.; Cheng, X.; Jiang, D.; Zafar, F. F.; Fu, Y.; Wang, S. Adsorption Modeling, Thermodynamics, and DFT Simulation of Tetracycline onto Mesoporous and High-Surface-Area NaOH-Activated Macroalgae Carbon. *J. Hazard. Mater.* **2022**, *425*, 127887.

(2) Chen, L.; Lang, H.; Liu, F.; Jin, S.; Yan, T. Presence of Antibiotics in Shallow Groundwater in the Northern and Southwestern Regions of China. *Groundwater* **2018**, *56* (3), 451−457.

(3) Chen, T.; Luo, L.; Deng, S.; Shi, G.; Zhang, S.; Zhang, Y.; Deng, O.; Wang, L.; Zhang, J.; Wei, L. Sorption of Tetracycline on H_3PO_4 Modified Biochar Derived from Rice Straw and Swine Manure. *Bioresour. Technol.* **2018**, *267*, 431−437.

(4) Xu, L.; Zhang, H.; Xiong, P.; Zhu, Q.; Liao, C.; Jiang, G. Occurrence, Fate, and Risk Assessment of Typical Tetracycline Antibiotics in the Aquatic Environment: A Review. *Sci. Total Environ.* **2021**, *753*, 141975.

(5) Vikesland, P. J.; Pruden, A.; Alvarez, P. J. J.; Aga, D.; Bürgmann, H.; Li, X. D.; Manaia, C. M.; Nambi, I.; Wigginton, K.; Zhang, T.; Zhu, Y. G. Toward a Comprehensive Strategy to Mitigate Dissemination of Environmental Sources of Antibiotic Resistance. *Environ. Sci. Technol.* **2017**, *51* (22), 13061−13069.

(6) Tang, J.; Ma, Y.; Deng, Z.; Li, P.; Qi, X.; Zhang, Z. One-Pot Preparation of Layered Double Oxides-Engineered Biochar for the Sustained Removal of Tetracycline in Water. *Bioresour. Technol.* **2023**, *381*, 129119.

(7) Liu, L.; Zhao, X.; Ding, G.; Han, C.; Liu, J. Fe_3N Sites Anchored Reduced Graphene Oxide Activate Peroxymonosulfate via Singlet Oxygen Dominated Process: Performance and Mechanisms. *Chem. Eng. J.* **2023**, *470*, 143820.

(8) Guo, X.; Wang, P.; Li, Y.; Zhong, H.; Li, P.; Zhang, C.; Zhao, T. Effect of Copper on the Removal of Tetracycline from Water by Myriophyllum Aquaticum: Performance and Mechanisms. *Bioresour. Technol.* **2019**, *291*, 121916.

(9) Wang, M.; Wang, Y.; Li, Y.; Wang, C.; Kuang, S.; Ren, P.; Xie, B. Persulfate Oxidation of Tetracycline, Antibiotic Resistant Bacteria,

and Resistance Genes Activated by Fe Doped Biochar Catalysts: Synergy of Radical and Non-Radical Processes. *Chem. Eng. J.* **2023**, *464*, 142558.
(10) Guo, J.; Huang, M.; Gao, P.; Zhang, Y.; Chen, H.; Zheng, S.; Mu, T.; Luo, X. Simultaneous Robust Removal of Tetracycline and Tetracycline Resistance Genes by a Novel UiO/TPU/PSF Forward Osmosis Membrane. *Chem. Eng. J.* **2020**, *398*, 125604.
(11) Teng, Y.; Li, W.; Wang, J.; Jia, S.; Zhang, H.; Yang, T.; Li, X.; Li, L.; Wang, C. A Green Hydrothermal Synthesis of Polyacrylonitrile@carbon/MIL-101(Fe) Composite Nanofiber Membrane for Efficient Selective Removal of Tetracycline. *Sep. Purif. Technol.* **2023**, *315*, 123610.
(12) Zheng, H.; Ji, Y.; Li, S.; Li, W.; Ma, J.; Niu, J. Ecotoxicity and Resistance Genes Induction Changing of Antibiotic Tetracycline Degradation Products Dominated by Differential Free Radicals. *Environ. Res.* **2023**, *227*, 115427.
(13) Zheng, W.; Liu, Y.; Liu, F.; Wang, Y.; Ren, N.; You, S. Atomic Hydrogen in Electrocatalytic Systems: Generation, Identification, and Environmental Applications. *Water Res.* **2022**, *223*, 118994.
(14) Wang, L.; Liu, Y.; Pang, D.; Song, H.; Zhang, S. Simultaneous Electrochemical Degradation of Tetracycline and Metronidazole through a High-Efficiency and Low-Energy-Consumption Advanced Oxidation Process. *Chemosphere* **2022**, *292*, 133469.
(15) Chen, X.; Shen, W.; Chen, J.; Zhu, Y.; Chen, C.; Xie, S. Tetracycline Biotransformation by a Novel Bacterial Strain Alcaligenes Sp. T17. *Sci. Total Environ.* **2022**, *832*, 155130.
(16) Huang, W. H.; Dong, C. D.; Chen, C. W.; Surampalli, R. Y.; Kao, C. M. Application of Sulfate Reduction Mechanisms for the Simultaneous Bioremediation of Toluene and Copper Contaminated Groundwater. *Int. Biodeterior. Biodegrad.* **2017**, *124*, 215−222.
(17) Zhou, B. Q.; Sang, Q. Q.; Wang, Y. J.; Huang, H.; Wang, F. J.; Yang, R. C.; Zhao, Y. T.; Xiao, Z. J.; Zhang, C. Y.; Li, H. P. Comprehensive Understanding of Tetracycline Hydrochloride Adsorption Mechanism onto Biochar-Based Gel Pellets Based on the Combination of Characterization-Based and Approximate Site Energy Distribution Methods. *J. Cleaner Prod.* **2023**, *416*, 137909.
(18) Zeng, H.; Li, J.; Xu, J.; Qi, W.; Hao, R.; Gao, G.; Lin, D.; Li, D.; Zhang, J. Preparation of Magnetic N-Doped Iron Sludge Based Biochar and Its Potential for Persulfate Activation and Tetracycline Degradation. *J. Cleaner Prod.* **2022**, *378*, 134519.
(19) Zhao, Q.; Yin, W.; Long, C.; Jiang, Z.; Jiang, J.; Yang, H. Insights into the Adsorption Behaviour and Mechanism of Tetracycline on Rectorite Mineral: Influence of Surface and Structure Evolution. *Appl. Clay Sci.* **2022**, *229*, 106698.
(20) Mengting, Z.; Kurniawan, T. A.; Avtar, R.; Othman, M. H. D.; Ouyang, T.; Yujia, H.; Xueting, Z.; Setiadi, T.; Iswanto, I. Applicability of TiO_2(B) Nanosheets@hydrochar Composites for Adsorption of Tetracycline (TC) from Contaminated Water. *J. Hazard. Mater.* **2021**, *405*, 123999.
(21) Li, C.; Zhang, X.; Wen, S.; Xiang, R.; Han, Y.; Tang, W.; Yue, T.; Li, Z. Interface Engineering of Zeolite Imidazolate Framework-8 on Two-Dimensional Al-metal-organic Framework Nanoplates Enhancing Performance for Simultaneous Capture and Sensing Tetracyclines. *J. Hazard. Mater.* **2020**, *395*, 122615.
(22) Wang, T.; Meng, Z.; Jiang, H.; Sun, X.; Jiang, L. Coexisting TiO_2 Nanoparticles Influencing Adsorption/ Desorption of Tetracycline on Magnetically Modified Kaolin. *Chemosphere* **2021**, *263*, 128106.
(23) Chang, P. H.; Mukhopadhyay, R.; Sarkar, B.; Mei, Y. C.; Hsu, C. H.; Tzou, Y. M. Insight and Mechanisms of Tetracycline Adsorption on Sodium Alginate/Montmorillonite Composite Beads. *Appl. Clay Sci.* **2023**, *245*, 107127.
(24) Liu, J.; Lin, Q.; Gao, J.; Jia, X.; Cai, M.; Liang, Q. Adsorption Properties and Mechanisms of Methylene Blue and Tetracycline by Nano-Silica Biochar Composites Activated by KOH. *Chemosphere* **2023**, *337*, 139395.
(25) Yin, K.; Wang, J.; Tian, X.; Yu, N.; Zhang, X.; Zhao, Y.; Liu, Y.; Sui, S.; Wang, C.; Lian, F.; Zhai, S.; Li, X.; Xing, B. Effect of Biochar-Derived Dissolved Organic Matter on Tetracycline Sorption by $KMnO_4$-Modified Biochar. *Chem. Eng. J.* **2023**, *474*, 145872.
(26) Nguyen, T. B.; Nguyen, T. K. T.; Chen, W. H.; Chen, C. W.; Bui, X. T.; Patel, A. K.; Dong, C. Di. Hydrothermal and Pyrolytic Conversion of Sunflower Seed Husk into Novel Porous Biochar for Efficient Adsorption of Tetracycline. *Bioresour. Technol.* **2023**, *373*, 128711.
(27) Qi, L.; Li, F. Y.; Huang, Z.; Jiang, P.; Baoyin, T.; Wang, H. Phytolith-Occluded Organic Carbon as a Mechanism for Long-Term Carbon Sequestration in a Typical Steppe: The Predominant Role of Belowground Productivity. *Sci. Total Environ.* **2017**, *577*, 413−417.
(28) Hodson, M. J. The Development of Phytoliths in Plants and Its Influence on Their Chemistry and Isotopic Composition. Implications for Palaeoecology and Archaeology. *J. Archaeol. Sci.* **2016**, *68*, 62−69.
(29) Puppe, D.; Kaczorek, D.; Stein, M.; Schaller, J. Silicon in Plants: Alleviation of Metal(Loid) Toxicity and Consequential Perspectives for Phytoremediation. *Plants* **2023**, *12* (13), 2407.
(30) Jais, F. M.; Chee, C. Y.; Ismail, Z.; Ibrahim, S. Experimental Design via NaOH Activation Process and Statistical Analysis for Activated Sugarcane Bagasse Hydrochar for Removal of Dye and Antibiotic. *J. Environ. Chem. Eng.* **2021**, *9* (1), 104829.
(31) Wu, F. C.; Tseng, R. L. High Adsorption Capacity NaOH-Activated Carbon for Dye Removal from Aqueous Solution. *J. Hazard. Mater.* **2008**, *152* (3), 1256−1267.
(32) Chen, S.; Zhang, B.; Xia, Y.; Chen, H.; Chen, G.; Tang, S. Influence of Mixed Alkali on the Preparation of Edible Fungus Substrate Porous Carbon Material and Its Application for the Removal of Dye. *Colloids Surf., A* **2021**, *609*, 125675.
(33) Regmi, P.; Garcia Moscoso, J. L.; Kumar, S.; Cao, X.; Mao, J.; Schafran, G. Removal of Copper and Cadmium from Aqueous Solution Using Switchgrass Biochar Produced via Hydrothermal Carbonization Process. *J. Environ. Manage.* **2012**, *109*, 61−69.
(34) Nguyen, A. T. Q.; Nguyen, A. M.; Nguyen, L. N.; Nguyen, H. X.; Tran, T. M.; Tran, P. D.; Dultz, S.; Nguyen, M. N. Effects of CO_2 and Temperature on Phytolith Dissolution. *Sci. Total Environ.* **2021**, *772*, 145469.
(35) Wang, T.; Xue, L.; Liu, Y.; Zhang, L.; Xing, B. N Self-Doped Hierarchically Porous Carbon Derived from Biomass as an Efficient Adsorbent for the Removal of Tetracycline Antibiotics. *Sci. Total Environ.* **2022**, *822*, 153567.
(36) Sun, J.; Ji, L.; Han, X.; Wu, Z.; Cai, L.; Guo, J.; Wang, Y. Mesoporous Activated Biochar from Crab Shell with Enhanced Adsorption Performance for Tetracycline. *Foods* **2023**, *12* (5), 1042.
(37) Zhuo, S. N.; Dai, T. C.; Ren, H. Y.; Liu, B. F. Simultaneous Adsorption of Phosphate and Tetracycline by Calcium Modified Corn Stover Biochar: Performance and Mechanism. *Bioresour. Technol.* **2022**, *359*, 127477.
(38) Yang, Q.; Wu, P.; Liu, J.; Rehman, S.; Ahmed, Z.; Ruan, B.; Zhu, N. Batch Interaction of Emerging Tetracycline Contaminant with Novel Phosphoric Acid Activated Corn Straw Porous Carbon: Adsorption Rate and Nature of Mechanism. *Environ. Res.* **2020**, *181*, 108899.
(39) Zhang, P.; Li, Y.; Cao, Y.; Han, L. Characteristics of Tetracycline Adsorption by Cow Manure Biochar Prepared at Different Pyrolysis Temperatures. *Bioresour. Technol.* **2019**, *285*, 121348.
(40) Qiao, X. Q.; Hu, F. C.; Tian, F. Y.; Hou, D. F.; Li, D. S. Equilibrium and Kinetic Studies on MB Adsorption by Ultrathin 2D MoS_2 Nanosheets. *RSC Adv.* **2016**, *6* (14), 11631−11636.
(41) Guan, W.; Pan, J.; Ou, H.; Wang, X.; Zou, X.; Hu, W.; Li, C.; Wu, X. Removal of Strontium(II) Ions by Potassium Tetratitanate Whisker and Sodium Trititanate Whisker from Aqueous Solution: Equilibrium, Kinetics and Thermodynamics. *Chem. Eng. J.* **2011**, *167* (1), 215−222.
(42) Mei, Y.; Xu, J.; Zhang, Y.; Li, B.; Fan, S.; Xu, H. Effect of Fe-N Modification on the Properties of Biochars and Their Adsorption Behavior on Tetracycline Removal from Aqueous Solution. *Bioresour. Technol.* **2021**, *325*, 124732.

https://doi.org/10.1021/acsomega.3c09049
ACS Omega 2024, 9, 8287−8296

(43) Liang, J.; Fang, Y.; Luo, Y.; Zeng, G.; Deng, J.; Tan, X.; Tang, N.; Li, X.; He, X.; Feng, C.; Ye, S. Magnetic Nanoferromanganese Oxides Modified Biochar Derived from Pine Sawdust for Adsorption of Tetracycline Hydrochloride. *Environ. Sci. Pollut. Res.* **2019**, *26* (6), 5892−5903.
(44) Xiang, W.; Wan, Y.; Zhang, X.; Tan, Z.; Xia, T.; Zheng, Y.; Gao, B. Adsorption of Tetracycline Hydrochloride onto Ball-Milled Biochar: Governing Factors and Mechanisms. *Chemosphere* **2020**, *255*, 127057.
(45) Xiang, Y.; Xu, Z.; Wei, Y.; Zhou, Y.; Yang, X.; Yang, Y.; Yang, J.; Zhang, J.; Luo, L.; Zhou, Z. Carbon-Based Materials as Adsorbent for Antibiotics Removal: Mechanisms and Influencing Factors. *J. Environ. Manage.* **2019**, *237*, 128−138.
(46) Zhang, Y.; Liu, Q.; Yang, C.; Wu, S.; Cheng, J. Magnetic Aluminum-Based Metal Organic Framework as a Novel Magnetic Adsorbent for the Effective Removal of Minocycline from Aqueous Solutions. *Environ. Pollut.* **2019**, *255*, 113226.
(47) Dai, Y.; Li, J.; Shan, D. Adsorption of Tetracycline in Aqueous Solution by Biochar Derived from Waste Auricularia Auricula Dregs. *Chemosphere* **2020**, *238*, 124432.
(48) Wang, Y.; Xu, L.; Wei, F.; Ding, T.; Zhang, M.; Zhu, R. Insights into the Adsorption Mechanism of Tetracycline on Hierarchically Porous Carbon and the Effect of Nanoporous Geometry. *Chem. Eng. J.* **2022**, *437*, 135454.
(49) Zhang, Y.; Zhang, J.; Chen, K.; Shen, S.; Hu, H.; Chang, M.; Chen, D.; Wu, Y.; Yuan, H.; Wang, Y. Engineering Banana-Peel-Derived Biochar for the Rapid Adsorption of Tetracycline Based on Double Chemical Activation. *Resour., Conserv. Recycl.* **2023**, *190*, 106821.
(50) Shi, Q.; Wang, W.; Zhang, H.; Bai, H.; Liu, K.; Zhang, J.; Li, Z.; Zhu, W. Porous Biochar Derived from Walnut Shell as an Efficient Adsorbent for Tetracycline Removal. *Bioresour. Technol.* **2023**, *383*, 129213.
(51) Yang, J.; Dai, J.; Wang, L.; Ge, W.; Xie, A.; He, J.; Yan, Y. Ultrahigh Adsorption of Tetracycline on Willow Branche-Derived Porous Carbons with Tunable Pore Structure: Isotherm, Kinetics, Thermodynamic and New Mechanism Study. *J. Taiwan Inst. Chem. Eng.* **2019**, *96*, 473−482.

https://doi.org/10.1021/acsomega.3c09049
ACS Omega 2024, 9, 8287−8296